A Deployable Coplanar Waveguide CoCo Antenna

Haiyang Wang, Le Chang, *Senior Member, IEEE*, Yue Li, *Senior Member, IEEE*, Kunpeng Wei, *Senior Member, IEEE*, and Zhijun Zhang, *Fellow, IEEE*

***Abstract*—In this letter, a deployable coplanar waveguide (CPW) coaxial colinear (CoCo) antenna is proposed with full coverage in the H-plane. The antenna features an ultra-thin profile of only 0.1 mm with excellent deployability. The proposed antenna consists of eight units, which are connected through metal crossover lines. The top and bottom metal layers alternate as the inner and outer conductors of the CPW. Metal bridges are introduced to mitigate the open stopband (OSB) phenomenon, which also eliminates the undesired CPW slot mode. A planar choke is designed to eliminate the effects of unbalanced coaxial feeding, ensuring consistency between the measured and simulated results. The antenna was fabricated using flexible printed circuit (FPC) technology. Within the target 4.8 GHz to 4.9 GHz band, the measured S_{11} is below −10 dB, and the efficiency is about 80%. The average gain in the H-plane is 5.8 dBi. The antenna shows great potential for applications in unmanned aerial vehicles (UAVs) and other mobile communication devices.**

***Index Terms*—Coaxial colinear (CoCo) antenna, deployable, flexible printed circuit (FPC), full coverage in H-plane, open stopband (OSB).**

I. Introduction

With the development of wireless communication, the number of application scenarios for antennas is continuously increasing [1]. In some applications, there is very limited storage space available for antennas, for example, satellites or outdoor mobile communication devices such as unmanned aerial vehicles (UAVs). The deployable antennas which can significantly reduce the required storage space are suitable for these scenarios [2], [3], [4], [5], [6], [7], [8]. In addition, wind resistance is an important factor in the antenna design of UAVs [9]. Rolling up the antenna during movement helps reduce resistance. In a hovering state of UAVs, the antenna deploys to achieve communication. Therefore, it is necessary to design a deployable omnidirectional antenna for UAVs.

Previous deployable antennas are predominantly concentrated on achieving directional radiation without considering full coverage in the H-plane. While there have been numerous works on omnidirectional antennas [10], [11], [12], [13], [14], deployable antennas with H-plane coverage remain unexplored. The coaxial colinear (CoCo) antenna is a classic H-plane omnidirectional antenna [15], [16], [17]. Traditional CoCo antennas divide the coaxial cable into multiple segments with a length of half wavelength to switch the inner and outer currents [17]. However, this type of cable CoCo antenna is a 3-D structure, which does not allow for deployment.

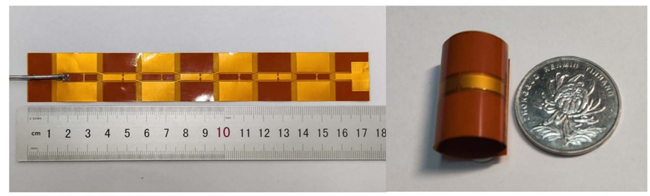

(a) (b)

Fig. 1. Photography of the antenna: (a) deployed state; (b) folded state.

Planar microstrip line CoCo antennas have been proposed [18], [19]. With the development of ultra-thin flexible printed circuit (FPC) technology, achieving a foldable microstrip line CoCo antenna seems possible. Nevertheless, the impedance of the microstrip line is significantly affected by the profile. With a low profile, the width of the microstrip line needs to be very small to maintain a characteristic impedance of 50 Ω, resulting in high losses in the microstrip line. Therefore, neither of the first two CoCo antennas can be deployable.

In addition to microstrip line CoCo antennas, coplanar waveguide (CPW) CoCo antennas are also planar structures. Compared to the former, the characteristic impedance of the latter is hardly affected by its profile. The characteristic impedance of CPW can be controlled by adjusting the distance between the inner and outer conductors. CPW CoCo antennas ensure in-phase current by switching between the inner and outer conductors. Based on this, a CPW CoCo antenna with a profile of 1 mm has been proposed [20]. However, this antenna cannot achieve bending and deployment functions. Besides, the antenna impedance bandwidth is narrow because it experiences the same open stopband (OSB) problem as leaky-wave antennas [21], [22], [23]. If the profile is further reduced, the OSB problem worsens, leading to a significant impedance mismatch. Additionally, the antenna connection parts are not compact enough. Therefore, designing a deployable CoCo antenna remains a challenge.

In this letter, we proposed a deployable CPW CoCo antenna based on FPC. The antenna has an ultrathin profile of only 0.1 mm. As shown in Fig. 1(a) and (b), the antenna can flexibly deploy and coil, significantly reducing the required storage space. The proposed antenna consists of two layers of metal

Manuscript received 12 June 2024; accepted 2 July 2024. Date of publication 5 July 2024; date of current version 8 October 2024. This work was supported by the National Natural Science Foundation of China under Grant 62271279. *(Corresponding author: Zhijun Zhang.)*

Haiyang Wang, Yue Li, and Kunpeng Wei are with the Department of Electronic Engineering, Tsinghua University, Beijing 100084, China, and also with the Beijing National Research Center for Information Science and Technology, Tsinghua University, Beijing 100084, China.

Le Chang is with the Shaanxi Key Laboratory of Deep Space Exploration Intelligent Information Technology, School of Information and Communications Engineering, Xi'an Jiaotong University, Xi'an 710049, China (e-mail: changle@xjtu.edu.cn).

Zhijun Zhang is with Xiaomi Communications Company Ltd., Beijing 100085, China (e-mail: zjzh@tsinghua.edu.cn).

Digital Object Identifier 10.1109/LAWP.2024.3423763

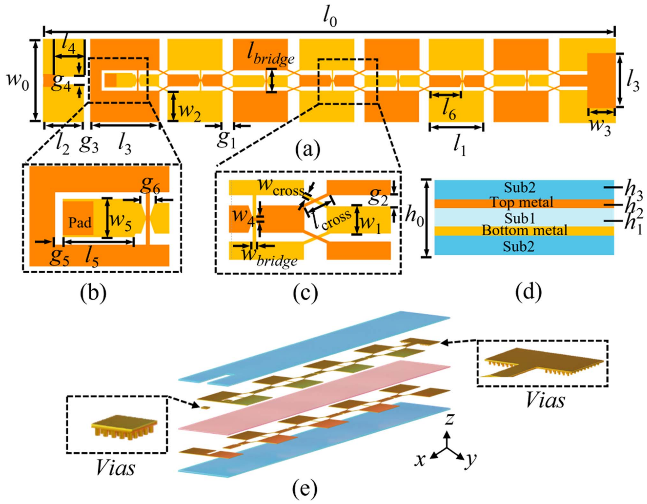

Fig. 2. Geometry of the proposed antenna. (a) Perspective view. (b) Localized enlarged view of the feed. (c) Localized enlarged view of the antenna unit. (d) Side view. (e) 3-D view.

TABLE I
DETAILED DIMENSIONS OF THE PROPOSED ANTENNA (UNIT: MM)

l_0	l_1	l_2	l_3	l_4	l_5	l_6	l_{bridge}	w_0
175	17	11.75	20.5	8.75	8.5	10.35	5	25
w_1	w_2	w_3	w_4	w_5	w_{cross}	w_{bridge}	g_1	g_2
3	10	8.5	8.75	3.8	0.2	0.28	3	1
g_3	g_4	g_5	g_6	h_0	h_1	h_2	h_3	
2.5	2	0.5	1.5	0.11	0.025	0.012	0.0275	

with a spacing of only 25 µm and three layers of dielectric. The antenna design includes metal crossover lines to periodically switch between inner and outer conductors, ensuring current in phase. Several metal bridges between outer conductors are introduced to simultaneously suppress OSB and CPW slot modes. The antenna easily covers the desired broadside frequency range of 4.8 GHz to 4.9 GHz, achieving full coverage in the H-plane with an average gain of 5.8 dBi. The proposed antenna exhibits excellent scalability for achieving a higher gain.

II. ANTENNA CONFIGURATION

Fig. 2 presents the geometry of the antenna, consisting of two layers of metal and three layers of dielectric. The substrate of Sub1 is Polyimide ($\varepsilon_r = 3.3$ and $\tan\delta = 0.01$) with a height of $h_1 = 25$ µm. The Sub2 is Polyimide ($\varepsilon_r = 2.9$ and $\tan\delta = 0.032$) with a height of $h_2 = 27$ µm. In this letter, we utilize a coaxial cable with the inner conductor connected to the bottom metal and the outer conductor connected to the top metal. Fig. 2(b) displays an enlarged image of the feed, where the top pad is connected to the bottom metal through metal vias. Fig. 2(e) represents the three-dimensional structure of the antenna. It should be noted that the metal vias are within Sub1. Here, for visualization, the metal vias are separated from Sub1. The planar structure on the left side of Fig. 2(a) is a planar choke structure. Detailed parameter configuration can be found in Table I. The antenna comprises eight radiating units interconnected by metal crossover lines. Switching of inner and outer conductors is achieved by crossover line. Metal bridges connect the two outer conductors of the CPW. At the end of the antenna, the inner and outer conductors shown in Fig. 2(e) are short-circuited using metal vias.

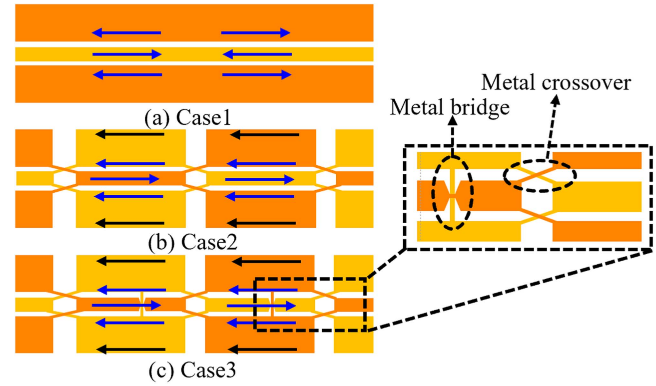

Fig. 3. Design process of the antenna (with partial units as representatives). (a) Case1. (b) Case2. (c) Case3 (proposed antenna).

III. ANTENNA DESIGN PROCESS

A. Radiation Principle of CoCo Antenna

To explain how the antenna works, the design process of the antenna is given in Fig. 3. The arrows represent the direction of the current. As shown in Fig. 3(a), Case1 is the CPW which transmits electromagnetic waves without radiation. The CPW is divided into several sections of identical units in Fig. 3(b). The inner conductor of the previous section becomes the outer conductor at this section, while the outer conductor of the previous section becomes the inner conductor at this section. The outer side current of each unit outer conductor remains uniform and in phase, achieving radiation with full coverage in the H-plane. Because of the need to ensure the flexibility of the antenna, the height of the Sub1 is only 25 µm. With such a low profile, the w_{cross} of the metal crossover lines must be small in Fig. 2(c). Otherwise, the upper and lower metal crossover lines will have a large overlap area, resulting in a strong capacitance. When the capacitance is large enough, a near short-circuit condition can be seen. The electromagnetic wave can hardly propagate to the next unit under this condition. Consequently, $w_{\text{cross}} = 0.2$ mm is finally selected. Because of the machining accuracy, linewidth below 0.2 mm is not considered.

B. Elimination of the Open Stopband

Since the length of each unit is approximately half the wavelength of the center frequency, the reflections of multiple metal crossover lines are superimposed in phase, leading to a rapid degradation of the impedance. This phenomenon is OSB. In Fig. 4, as h_1 gradually decreases, the reduced distance between the metal crossover lines leads to an increased value of the reflection coefficient, resulting in a more pronounced OSB phenomenon. Fig. 4 further reveals that as h_1 increases, the frequency associated with the OSB shifts to lower frequencies. This shift is attributed to the increase in h_1 for Sub1, resulting in a corresponding rise in effective permittivity. To suppress the OSB, we can introduce a second discontinuity in each unit to cancel out the original reflection caused by metal crossover lines between the two units. As shown in Fig. 3(c), the second discontinuity is introduced by a metal bridge that connects the

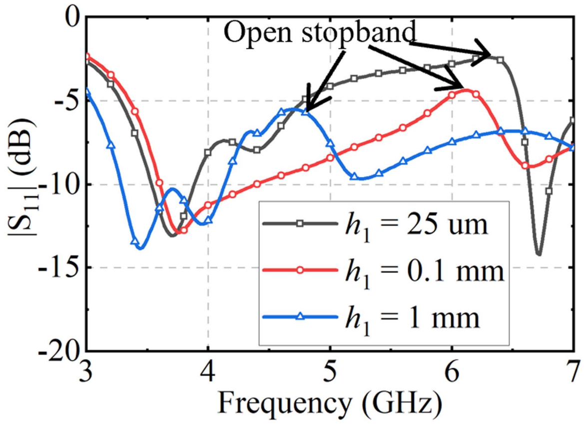

Fig. 4. Simulated S_{11} at different h_1.

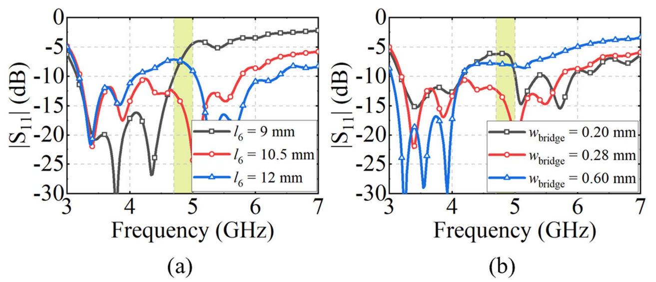

Fig. 5. Effect of parameters w_{bridge} and l_6 on S_{11}. (a) l_6 ($w_{\mathrm{bridge}} = 0.28$ mm). (b) w_{bridge} ($l_6 = 10.5$ mm).

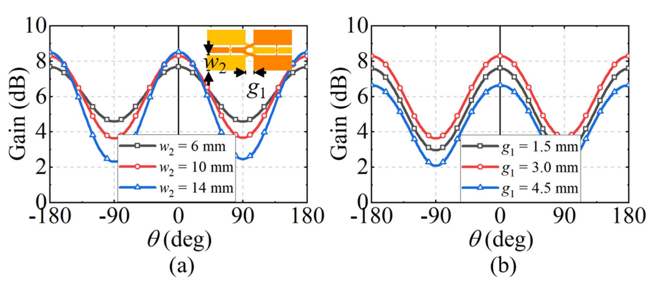

Fig. 6. Radiation patterns for (a) different values of w_2 with $g_1 = 3.0$ mm and (b) different values of g_1 with $w_2 = 10$ mm. (4.85 GHz, H-plane).

outer conductors on both sides. To decrease the amplitude of the reflection coefficient of the metal bridge, the width of the inner conductor is reduced from w_1 to w_4 near the metal bridge as shown in Fig. 2(c). In this article, the value of w_4 is 0.3 mm. We can adjust the values of l_6 and w_{bridge} to control the phase and amplitude of the second reflection, respectively. Fig. 5 shows the changes in $S_{11,}$ adjusting the parameters l_6 and w_{bridge}. Here, $l_6 = 10.5$ mm and $w_{\mathrm{bridge}} = 0.28$ mm are selected, achieving reflection cancellation of two discontinuities. It should be noted that the metal bridge not only suppresses the OSB but also eliminates the slot mode of the CPW.

Fig. 6 illustrates the influence of parameters w_2 and g_1 on the antenna radiation pattern. The value of w_2 directly affects the gain variation in the H-plane, as shown in Fig. 6(a). As the value of w_2 increases from 6 mm to 14 mm, the gain variation rises from 3 dB to 6.1 dB. It can be explained that the antenna is a two-element array in the H-plane. The array factor directional pattern is directly influenced by the value of w_2. For improved omnidirectionality, a smaller value of w_2 should be selected. Conversely, for higher gain at $\theta = 0°$, a larger value of w_2 is preferable. Here, $w_2 = 10$ mm is selected. Fig. 6(b) indicates that g_1 results in a change in the H-plane gain. This is because as g_1 varies from 1.5 mm to 4.5 mm, the angle of the maximum gain in the E-plane corresponds to $-4°$, $0°$, and $4°$, respectively. In other words, g_1 changes the period of the unit, causing a gradient in the phase distribution.

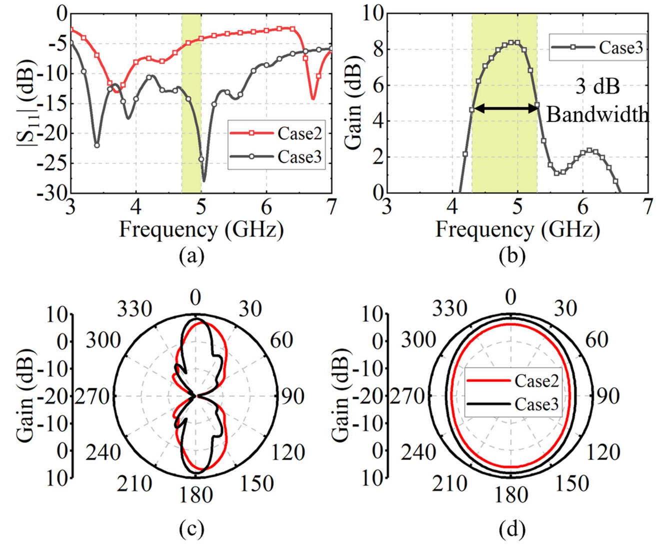

Fig. 7. S_{11} and gain for Case 2 and Case 3. (a) S_{11}. (b) 3 dB gain bandwidth. (c) Gain in the E-plane at 4.85 GHz (*xoz*). (d) Gain in the H-plane at 4.85 GHz (*yoz*).

C. Processing of the Terminal and Initial Units

The antenna consists of identical units except for the terminal and initial units. The last unit needs to be truncated, and the initial units require feedline matching. There is still a small portion of energy reflected at the terminal unit. The position of the short circuit point in the last unit is adjusted to control the phase of the reflected energy, achieving in-phase radiation to improve gain. Ultimately, $w_3 = 8.5$ mm is selected. Because the reflected energy constitutes a relatively small proportion, the antenna gain change is not significant. For the first unit of the antenna, we can adjust the distance between the inner and outer conductors (g_2) of the unit to achieve impedance matching.

The impedance matching and gain between Case 3 and Case 2 are depicted in Fig. 7. Fig. 7(a) presents that the impedance bandwidth is 3.2 GHz to 5.8 GHz. Case 3 effectively suppresses the OSB and thus significantly improves the impedance. In Fig. 7(b), we can observe that the 3 dB gain bandwidth is 4.3 GHz to 5.3 GHz. We define the 3 dB gain bandwidth as the frequency range where the broadside gain decreases by 3 dB from the maximum broadside gain. Overall, the proposed antenna can easily cover the 4.8 GHz to 4.9 GHz target broadside band. For a fair comparison, Fig. 7(c) and (d) represent the gain of two cases without considering the matching conditions. The gain of Case 3 was enhanced by 1.8 dB at $\theta = 0°$ compared to Case 2. From the current distribution in Fig. 8, it can be seen that Case 3 exhibits a more uniform radiation current distribution on the outer conductor, and each unit radiates in phase. Hence, the gain of the proposed antenna is improved.

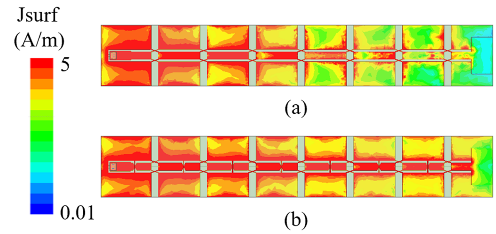

Fig. 8. Current complex amplitude distributions of the antenna at 4.85 GHz. (a) Case2. (b) Case3 (proposed).

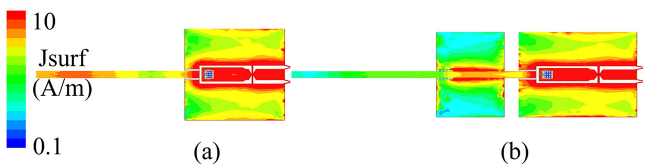

Fig. 9. Current distribution on the coaxial line. (a) Without planar choke and (b) with planar choke.

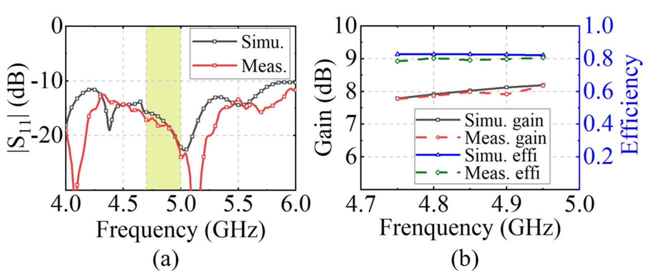

Fig. 10. Simulated and measured (a) S_{11} and (b) gains and efficiencies.

D. Planar Choke Design

Actually, the antenna is fed using a coaxial line. When coaxial feeding is added to the simulation software, the gain decreases by 0.7 dB compared to ideal port feeding. To eliminate the effects of unbalanced feeding, a planar choke structure has been designed and directly integrated into the dielectric. The planar choke is located on the bottom metal layer, as shown in Fig. 2(e). As shown in Fig. 9(a) and (b), the current on the outer conductor of the coaxial line significantly decreases. This is because the coaxial outer conductor and the planar choke structure form an open circuit at the feeding point.

IV. Simulated and Measured Results

To validate the performance of the proposed antenna, a prototype was fabricated using FPC technology as shown in Fig 1. Fig. 1(a) and (b) shows the antenna in its deployed and folded states, respectively.

A. Reflection Coefficient

The simulated and measured reflection coefficients are reported in Fig. 10(a). The discrepancy between the measured and simulated results is caused by the fabrication error. Overall, the simulated and measured S_{11} values are in good agreement across the entire frequency range. In the desired operating frequency range of 4.8 GHz to 4.9 GHz, the values closely match.

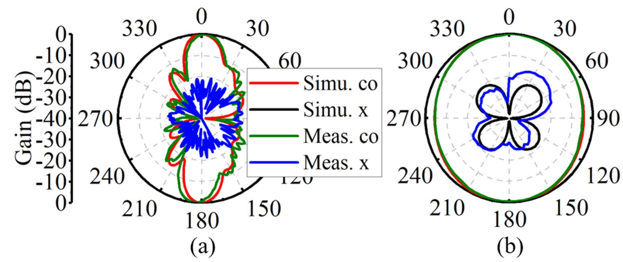

Fig. 11. Simulated and measured radiation patterns at 4.85 GHz. (a) E-plane. (b) H-plane.

TABLE II
Comparison of the Proposed Antenna and Previous Omnidirectional Antennas

Ref.	Antenna type	Footprint $\lambda_0 \times \lambda_0$ *	**Profile (mm)**	Gain (dBi)	Gain variation (dB)	**Deploy-able**
[12]	Planar Dipole	2.88 ×0.38	**0.8**	6.5	1.5	**No**
[17]	Cable CoCo	4.57 ×0.46	**4**	8.5	1	**No**
[20]	CPW CoCo	1.54 ×0.20	**1**	5.3	1.3	**No**
This work	CPW CoCo	2.82 ×0.40	**0.1**	8	4.6	**Yes**

* λ_0 is the wavelength of the free space.

B. Radiation Performance

The simulated and measured gains, efficiencies, and radiation patterns are shown in Figs. 10(b) and 11. Fig. 10(b) shows that the measured gain and efficiency of the fabricated antenna are generally close to the simulated results. The fabricated antenna maintains a gain of approximately 8 dBi and an efficiency of 80% within its operating frequency range. Fig. 11 indicates that the cross polarization in the E-plane and H-plane is relatively low. The simulated and measured results are consistent.

C. Discussion

Table II provides a comparison between our work and other omnidirectional antennas. In comparison to the planar dipole antenna in [12], the CoCo antenna requires only a simple coaxial feed without a complex feeding network, showing superior scalability. Compared to the previous CoCo antennas [17], [20], the profile of the proposed antenna based on FPC is only 0.1 mm, which has excellent deployability, significantly reducing the required storage space.

V. Conclusion

In this letter, a deployable CPW CoCo antenna with full coverage in H-plane is proposed. The antenna is designed to deploy during operation and fold up when not in use, reducing required storage space. The small separation distance of 25 µm between the two metal layers introduces a pronounced OSB phenomenon. Metal bridges are introduced to suppress the OSB and the slot mode of CPW, significantly improving the antenna impedance bandwidth and gain. Finally, using the FPC technology for manufacturing, the proposed antenna demonstrates outstanding deployability. Within the target frequency range of 4.8 GHz to 4.9 GHz, the average gain in the H-plane is 5.8 dBi with full H-plane coverage.

REFERENCES

[1] J. G. Andrews et al., “What will 5G Be?,” *IEEE J. Sel. Areas Commun.*, vol. 32, no. 6, pp. 1065–1082, Jun. 2014.

[2] Y. Rahmat-Samii, J. Wang, J. Zamora, G. Freebury, R. E. Hodges, and S. J. Horst, “A 7 m $\times$ 1.5 m aperture parabolic cylinder deployable mesh reflector antenna for next-generation satellite synthetic aperture radar,” *IEEE Trans. Antennas Propag*, vol. 71, no. 8, pp. 6378–6389, Aug. 2023.

[3] T. Takano et al., “Deployable antenna with 10-m maximum diameter for space use,” *IEEE Trans. Antennas Propag*, vol. 52, no. 1, pp. 2–11, Jan. 2004.

[4] N. Chahat, J. Sauder, R. Hodges, M. Thomson, Y. R. Samii, and E. Peral, “Ka-band high-gain mesh deployable reflector antenna enabling the first radar in a CubeSat: RainCube,” in *Proc. 10th Eur. Conf. Antennas Propag.*, Apr. 2016, pp. 1–4.

[5] B. Imaz-Lueje, M. R. Pino, and M. Arrebola, “Deployable multi-faceted reflectarray antenna in offset configuration with band enhancement,” *IEEE Trans. Antennas Propag*, vol. 70, no. 12, pp. 11686–11696, Dec. 2022.

[6] A. Guarriello, R. Loison, D. Bresciani, H. Legay, and G. Goussetis, “Structural and radio frequency co-design and optimization of large deployable reflectarrays for space missions,” *IEEE Trans. Antennas Propag*, vol. 71, no. 5, pp. 3916–3927, May 2023.

[7] Y. Cui, R. Bahr, S. A. Nauroze, T. Cheng, T. S. Almoneef, and M. M. Tentzeris, “3D printed ‘kirigami’-inspired deployable bi-focal beam-scanning dielectric reflectarray antenna for mm-wave applications,” *IEEE Trans. Antennas Propag*, vol. 70, no. 9, pp. 7683–7690, Sep. 2022.

[8] J. Liu, H. Lu, Z. Dong, Z. Liu, Y. Liu, and X. Lv, “Fully metallic dual-polarized Luneburg lens antenna based on gradient parallel plate waveguide loaded with nonuniform nail,” *IEEE Trans. Antennas Propag*, vol. 70, no. 1, pp. 697–701, Jan. 2022.

[9] K. Kawabata and H. Arai, “Wind influence of air wire antenna suspended from drone,” in *Proc. Int. Symp. Antennas Propag.*, Oct. 2018, pp. 1–2.

[10] Z. Zhou, Y. Li, Y. He, Z. Zhang, and P. Y. Chen, “A slender Fabry–Perot antenna for high-gain horizontally polarized omnidirectional radiation,” *IEEE Trans. Antennas Propag*, vol. 69, no. 1, pp. 526–531, Jan. 2021.

[11] L. Chang, Y. Li, Z. Zhang, and Z. Feng, “Horizontally polarized omnidirectional antenna array using cascaded cavities,” *IEEE Trans. Antennas Propag*, vol. 64, no. 12, pp. 5454–5459, Dec. 2016.

[12] J. H. Lu and Y. H. Liu, “Planar dual-band dipole array for long-term evolution/worldwide interoperability for microwave access points,” *Microw. Opt. Technol. Lett.*, vol. 54, pp. 811–815, 2012.

[13] K. Wei, Z. Zhang, Z. Feng, and M. F. Iskander, “A MNG-TL loop antenna array with horizontally polarized omnidirectional patterns,” *IEEE Trans. Antennas Propag*, vol. 60, no. 6, pp. 2702–2710, Jun. 2012.

[14] K. Wei, Z. Zhang, W. Chen, Z. Feng, and M. F. Iskander, “A triband shunt-fed omnidirectional planar dipole array,” *IEEE Antennas Wireless Propag. Lett*, vol. 9, pp. 850–853, 2010.

[15] T. J. Judasz and B. B. Balsley, “Improved theoretical and experimental models for the coaxial colinear antenna,” *IEEE Trans. Antennas Propag*, vol. 37, no. 3, pp. 289–296, Mar. 1989.

[16] Q. Wang, X. L. Yang, Y. T. Li, Z. B. Li, and S. T. Chen, “Design of a high gain and low sidelobe coaxial collinear antenna array,” in *Proc. Int. Conf. Comput. Problem-Solving*, Oct. 2011, pp. 26–28.

[17] A. Hosseini-Fahraji and M. Manteghi, “Design of a broadband high-gain end-fed coaxial collinear antenna,” *IEEE Antennas Wireless Propag. Lett*, vol. 20, no. 9, pp. 1770–1774, Jul. 2021.

[18] Z. Peng-Fei, S. Li-Ming, L. Yong, and L. Xin, “A novel omnidirectional microstrip coaxial collinear antenna array,” in *Proc. IET Int. Radar Conf.*, Apr. 2013, pp. 1–4.

[19] K. Wei, Z. Zhang, and Z. Feng, “Design of a dual-band omnidirectional planar microstrip antenna array,” *Prog. Electromagn. Res.*, vol. 126, pp. 101–120, 2012.

[20] X. Du, H. Li, and Y. Yin, “A board omnidirectional coplanar waveguide antenna with choke sleeve,” in *Proc. Int. Conf. Sensor Netw. Signal Process.*, Oct. 2018, pp. 370–374.

[21] S. Otto, A. Al-Bassam, A. Rennings, K. Solbach, and C. Caloz, “Transversal asymmetry in periodic leaky-wave antennas for Bloch impedance and radiation efficiency equalization through broadside,” *IEEE Trans. Antennas Propag*, vol. 62, no. 10, pp. 5037–5054, Oct. 2014.

[22] K. Wei, Z. Zhang, Z. Feng, and M. F. Iskander, “Periodic leaky-wave antenna array with horizontally polarized omnidirectional pattern,” *IEEE Trans. Antennas Propag*, vol. 60, no. 7, pp. 3165–3173, Jul. 2012.

[23] S. Paulotto, P. Baccarelli, F. Frezza, and D. R. Jackson, “A novel technique for open-stopband suppression in 1-D periodic printed leaky-wave antennas,” *IEEE Trans. Antennas Propag*, vol. 57, no. 7, pp. 1894–1906, Jul. 2009.